NUMERICAL ANALYSIS OF DRAG COEFFICIENTS AND MASS TRANSFER OF TWO ADJACENT SPHERES

IZUMI TANIGUCHI AND KOICHI ASANO
Department of Chemical Engineering, Tokyo Institute of Technology, Tokyo 152

Key Words: Atomization, Mass Transfer, Numerical Analysis, Finite Difference Method, Two Sphere, Drag Coefficient, Evaporation

Numerical analysis of the drag coefficients and the diffusion fluxes of two coaxially arranged spheres was made by use of a finite difference method with bipolar coordinate system for $Re_p=1-30$, $L/D_A=1.50-9.99$ and $Sc=1.0$. The present numerical data were compared with existing numerical and experimental data and showed good agreement. New correlations for the effect of the distance between two spheres on the drag coefficients and the diffusion fluxes of the two spheres were proposed. Measurements of rates of evaporation of a pendant water drop in the presence of a coaxially arranged inert solid sphere into dry air were made for $Re_p=30$ and the data were compared with numerical data.

Introduction

Motion, heat and mass transfer of two adjacent liquid drops are fundamental problems for the study of transport phenomena in spray systems, such as spray drying, quenching or combustion of liquid fuel. Although many theoretical or experimental approaches to drag coefficients and heat and mass transfer of a single drop have been made in recent decades, relatively few works are known that deal with two adjacent drops. Some theoretical approaches to this problem have been made recently, but most are concerned with those in the low Reynolds number range[1,14,15] or those for quiescent fluid.[7,9,11,12,16] Few works except that of Tal *et al.*[15] deal with the intermediate Reynolds number range, which is important for practical application.

In our previous paper[2] an experimental approach was made to the effect of an adjacent solid sphere on the rates of evaporation of a volatile pendant drop in the intermediate Reynolds number range. The purpose of the present work is to make a theoretical approach to the drag coefficients and the rates of mass transfer of coaxially arranged solid spheres of the same diameter for the low-to-intermediate Reynolds number range and to compare it with observed data.

1. Numerical Analysis

1.1 Governing equations

Figure 1 shows the bipolar grid system[6] employed in the present calculation, where R_A and R_B are the radii of the two solid spheres. The direction of free stream is parallel to the axis connecting the center of the two spheres.

The Navier-Stokes equation and the diffusion equation for steady, incompressible, axisymmetric flow of constant physical properties in terms of dimensionless stream function, ψ, in bipolar coordinates (η, ξ) can be written as:

$$\sin\xi\cdot(\cosh\eta-\cos\xi)\cdot\left(\frac{\partial\psi}{\partial\eta}\cdot\frac{\partial}{\partial\xi}-\frac{\partial\psi}{\partial\xi}\cdot\frac{\partial}{\partial\eta}\right)\cdot\frac{(\cosh\eta-\cos\xi)^2}{\sin^2\xi}E^2\psi=\frac{1}{Re_c}E^2(E^2\psi) \tag{1}$$

where

$$E^2=(\cosh\eta-\cos\xi)\cdot\left[\frac{(1-\cos\xi\cdot\cosh\eta)}{\sin\xi}\cdot\frac{\partial}{\partial\xi}+(\cosh\eta-\cos\xi)\cdot\frac{\partial^2}{\partial\xi^2}+\sinh\eta\cdot\frac{\partial}{\partial\eta}+(\cosh\eta-\cos\xi)\cdot\frac{\partial^2}{\partial\eta^2}\right] \tag{2}$$

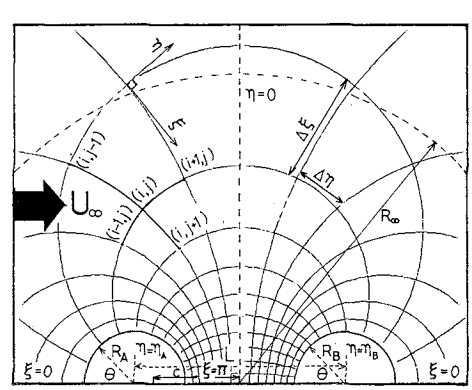

Fig. 1. Bipolar grid system.

Received October 4, 1986. Correspondence concerning this article should be addressed to K. Asano.

and

$$\frac{\partial\psi}{\partial\eta}\frac{\partial\theta_c}{\partial\xi}-\frac{\partial\psi}{\partial\xi}\frac{\partial\theta_c}{\partial\eta}=\frac{1}{Re_cSc}\left\{-\frac{\sin\xi\sinh\eta}{(\cosh\eta-\cos\xi)^2}\frac{\partial\theta_c}{\partial\eta}+\frac{\cos\xi\cosh\eta-1}{(\cosh\eta-\cos\xi)^2}\frac{\partial\theta_c}{\partial\xi}+\frac{\sin\xi}{\cosh\eta-\cos\xi}\frac{\partial^2\theta_c}{\partial\eta^2}+\frac{\sin\xi}{\cosh\eta-\cos\xi}\frac{\partial^2\theta_c}{\partial\xi^2}\right\} \tag{3}$$

The diameters of the two spheres and the focus of the bipolar coordinates can be expressed in terms of bipolar coordinates as follows:

$$D_A=2c/|\sinh\eta_A| \tag{4}$$

$$D_B=2c/|\sinh\eta_B| \tag{5}$$

$$c=L/(1/|\tanh\eta_A|+1/|\tanh\eta_B|) \tag{6}$$

The dimensionless orthogonal coordinates η and ξ can be expressed in terms of ordinary rectangular coordinates (X, Y) as follows:

$$X=c\sinh\eta/(\cosh\eta-\cos\xi) \tag{7}$$

$$Y=c\sin\xi/(\cosh\eta-\cos\xi) \tag{8}$$

All terms in Eqs. (1)–(3) have been made in dimensionless form by the following relations:

$$\psi=\psi'/c^2U_\infty \tag{9a}$$

$$\zeta=\zeta' c/U_\infty \tag{9b}$$

$$E^2=c^2E'^2 \tag{9c}$$

$$Re_c=cU_\infty/\nu \tag{9d}$$

The relation between Re_c and drop Reynolds number of the front sphere is given by the following equation:

$$Re_p=D_AU_\infty/\nu=\frac{2}{|\sinh\eta_A|}\cdot Re_c \tag{10}$$

Equation (1), a fourth-order partial differential equation, can be reduced to two simultaneous second-order equations by introducing the dimensionless vorticity, ζ, as follows:

$$E^2\psi=\zeta\sin\xi/(\cosh\eta-\cos\xi) \tag{11}$$

The boundary conditions for Eqs. (1), (3) and (11) are given by:

$$\xi=0 \quad : \quad \psi=0 \tag{12a}$$

$$\zeta=0 \tag{12b}$$

$$\partial\theta_c/\partial\xi=0 \tag{12c}$$

$$\xi=\pi \quad : \quad \psi=0 \tag{12d}$$

$$\zeta=0 \tag{12e}$$

$$\partial\theta_c/\partial\xi=0 \tag{12f}$$

$$\eta=\eta_A,\eta_B \ : \quad \psi=0 \tag{12g}$$

$$\zeta=(\cosh\eta-\cos\xi)\cdot E^2\psi/\sin\xi \tag{12h}$$

$$\theta_c=1 \tag{12i}$$

Outer boundary $X=R_\infty$

$$\psi=\sin^2\xi/2(\cosh\eta-\cos\xi)^2 \tag{12j}$$

$$\zeta=0 \tag{12k}$$

$$\theta_c=0 \tag{12l}$$

The outer boundary of the grid system, R_∞, is taken as three times the dimensionless distance between the front stagnation point of the front sphere and the rear stagnation of the rear sphere,

$$R_\infty=\frac{R'_\infty}{c}=\frac{3(R_A+R_B+L)}{c}=6(\cosh\eta_A+1)/|\sinh\eta_A| \tag{13}$$

according to a suggestion by Tal *et al.*[15]

1.2 Method of calculation

Equations (1), (3) and (11) with (12) were solved numerically by a finite difference method with relaxation technique.[13] The finite difference form of Equations (1), (11) and (3) are shown in the **Appendix**.

The optimum relaxation coefficients for the calculaion of the Navier-Stokes equation and the diffusion equation were chosen by a trial-and-error method for each sphere spacing and Reynolds number. The initial values for the stream functions were calculated from an analytical solution under creeping flow condition.[14]

The calculation of the stream function was made until either of the following convergence criteria was satisfied.

$$\left|\frac{\psi_{i,j}^{n+1}-\psi_{i,j}^{n}}{\psi_{i,j}^{n+1}}\right|<10^{-6} \tag{14}$$

$$\left|\frac{\psi_{i,j}^{n+1}-\psi_{i,j}^{n}}{\psi_{i,j}^{n+1}+1}\right|<10^{-7} \tag{15}$$

The calculation of the diffusion equation was made until either of the following convergence criteria was satisfied.

$$\left|\frac{\theta_{c_{i,j}}^{k+1}-\theta_{c_{i,j}}^{k}}{\theta_{c_{i,j}}^{k}}\right|<\varepsilon_1 \tag{16}$$

$$|\theta_{c_{i,j}}^{k+1}-\theta_{c_{i,j}}^{k}|<\varepsilon_2 \tag{17}$$

where

$$\varepsilon_1=10^{-5}\text{–}10^{-6} \quad \text{and} \quad \varepsilon_2=10^{-6}\text{–}10^{-7} \tag{18}$$

Ranges of variables for the calculation are shown in **Table 1**.

Table 1. Ranges of variables for the present calculation

Re_p	L/D_A	Sc	R_∞	M	N	$\Delta\eta$	$\Delta\xi$	η_A
1	1.50	1.0	14.0	81	61	0.024	$\pi/60$	−0.962
	2.00	1.0	11.0	81	61	0.033	$\pi/60$	−1.317
	4.00	1.0	8.0	81	61	0.052	$\pi/60$	−2.063
	5.99	1.0	7.0	81	61	0.062	$\pi/60$	−2.477
	9.99	1.0	6.0	81	61	0.075	$\pi/60$	−2.992
10	1.50	1.0	14.0	81	61	0.024	$\pi/60$	−0.962
	2.00	1.0	11.0	81	61	0.033	$\pi/60$	−1.317
	4.00	1.0	8.0	81	61	0.052	$\pi/60$	−2.063
	5.99	1.0	7.0	81	61	0.062	$\pi/60$	−2.477
	9.99	1.0	6.0	81	61	0.075	$\pi/60$	−2.992
20	1.50	1.0	14.0	81	61	0.024	$\pi/60$	−0.962
	2.00	1.0	11.0	81	61	0.033	$\pi/60$	−1.317
	4.00	1.0	8.0	81	61	0.052	$\pi/60$	−2.063
	5.99	1.0	7.0	81	61	0.062	$\pi/60$	−2.477
	9.99	1.0	6.0	81	61	0.075	$\pi/60$	−2.992
30	1.50	1.0	14.0	101	61	0.019	$\pi/60$	−0.962
	4.00	1.0	8.0	101	61	0.041	$\pi/60$	−2.063
	9.99	1.0	6.0	101	61	0.060	$\pi/60$	−2.992

1.3 Calculation of drag coefficients and diffusion fluxes

The pressure distributions on the surface of the spheres can be calculated from the surface vorticities by the following equation.

Front spheres:

$$P_A=1+\frac{4}{Re_c}\int_{\eta_A}^{\eta_{A\infty}}\left(\frac{\partial\zeta}{\partial\xi}\right)_{\xi=0}d\eta + \frac{2}{Re_c}\int_0^{\xi}\left\{\frac{\partial\zeta}{\partial\eta}-\frac{\zeta\sinh\eta_A}{\cosh\eta_A-\cos\xi}\right\}_{\eta=\eta_A}d\xi \tag{19}$$

Rear sphere:

$$P_B=P_{\eta=\eta_A,\xi=\pi}-\frac{4}{Re_c}\int_{\eta_B}^{\eta_A}\left(\frac{\partial\zeta}{\partial\xi}\right)_{\xi=\pi}d\eta + \frac{2}{Re_c}\int_{\pi}^{\xi}\left\{\frac{\partial\zeta}{\partial\eta}-\frac{\zeta\sinh\eta}{\cosh\eta_B-\cos\xi}\right\}_{\eta=\eta_B}d\xi \tag{20}$$

The form drag coefficients of the spheres can be calculated from the surface pressure distributions and the surface vorticities by the following equations.

Front sphere:

$$C_{DPA}=2|\sinh\eta_A|^2\int_0^{\pi}\frac{P_A\sin\xi(\cos\xi\cosh\eta_A-1)}{(\cosh\eta_A-\cos\xi)^3}d\xi \tag{21}$$

Rear sphere:

$$C_{DPB}=-2|\sinh\eta_B|^2\int_0^{\pi}\frac{P_B\sin\xi(\cos\xi\cosh\eta_B-1)}{(\cosh\eta_B-\cos\xi)^3}d\xi \tag{22}$$

The friction drag coefficients of the spheres can be calculated from the surface vorticities by the following equations.

Front sphere:

$$C_{DFA}=-\frac{4|\sinh\eta_A|^2\sinh\eta_A}{Re_c}\times\int_0^{\pi}\frac{\sin^2\xi}{(\cosh\eta_A-\cos\xi)^3}\zeta\Big|_{\eta=\eta_A}d\xi \tag{23}$$

Rear sphere:

$$C_{DFB}=\frac{4|\sinh\eta_B|^2\sinh\eta_B}{Re_c}\int_0^{\pi}\frac{\sin^2\xi}{(\cosh\eta_B-\cos\xi)^3}\zeta\Big|_{\eta=\eta_B}d\xi \tag{24}$$

Total drag coefficients can be calculated by the following equations:

$$C_D=C_{DP}+C_{DF} \tag{25}$$

The local diffusion fluxes on the surface of the spheres can be calculated from the concentration profiles by use of the following equations.

Front sphere:

$$Sh_{\eta_A}(1-\omega_s)=-\frac{2(\cosh\eta_A-\cos\xi)}{|\sinh\eta_A|}\frac{\partial\theta_c}{\partial\eta}\Big|_{\eta=\eta_A} \tag{26}$$

Rear sphere:

$$Sh_{\eta_B}(1-\omega_s)=-\frac{2(\cosh\eta_B-\cos\xi)}{|\sinh\eta_B|}\frac{\partial\theta_c}{\partial\eta}\Big|_{\eta=\eta_B} \tag{27}$$

The average diffusion fluxes over the surface of the spheres can be calculated as follows.

Front sphere:

$$Sh_A(1-\omega_s)=-|\sinh\eta_A|\times\int_0^{\pi}\frac{\sin\xi}{\cosh\eta_A-\cos\xi}\frac{\partial\theta_c}{\partial\eta}\Big|_{\eta=\eta_A}d\xi \tag{28}$$

Rear sphere:

$$Sh_B(1-\omega_s)=-|\sinh\eta_B|\times\int_0^{\pi}\frac{\sin\xi}{\cosh\eta_B-\cos\xi}\frac{\partial\theta_c}{\partial\eta}\Big|_{\eta=\eta_B}d\xi \tag{29}$$

Calculations were made with a HITAC M-280H computer. The CPU time for calculation of the Navier-Stokes equation and the diffusion equation were about 120 min. and 90 min., respectively.

2. Drag Coefficients of Two Coaxially Arranged Solid Spheres

2.1 Drag coefficients of front sphere for the case of large coaxial distance

The drag coefficients of the front sphere will approach those for single spheres if the distances be-

tween the two spheres become large. To confirm the validity of the present calculation the drag coefficients of the front sphere at $L/D_A=9.99$ were calculated and compared with those for single spheres. **Figure 2** shows the results of the comparison. The solid line in the figure is the well-known Lapple-Shepherd correlation[8] for single solid spheres and the dot-dash line is the one by Clift *et al.*[5] Good agreement between the present calculation and the empirical correlation for single spheres is observed.

The front stagnation pressures of the front sphere also showed good agreement with those for single solid sphere.[3] These facts may indicate the validity of the present calculation.

2.2 Flow field around two adjacent solid spheres

Figures 3(a) and **(b)** show the stream lines around two coaxially arranged solid spheres for the case where the distance between the two spheres is quite small ($L/D_A=1.5$) but at different Reynolds numbers, $Re_p=1$ and 30, respectively. For the low Reynolds number range (Figure 3a) the stream lines are almost symmetric with respect to the median point connecting the two spheres. But for intermediate Reynolds number range (Figure 3b), separation of flow is observed in the region between the two spheres and stream lines are not symmetrical.

The stream lines for the case of large distances between the two spheres showed similar profiles to those for single spheres.

Figure 4 shows an example of local distributions of the surface pressures of the front (dotted lines) and the rear (solid lines) spheres for various L/D_A and at $Re_p=1.0$. The figure indicates that the surface pressures of the front sphere are little affected by the presence of the rear sphere for the upper-half region and only a mild effect is observed in the lower-half region if the distances between the spheres becomes small. But for the rear sphere the effect becomes much more considerable as L/D_A increases.

2.3 Form-, friction- and total-drag coefficients of the front and the rear spheres

Figure 5 shows the effect of distances between the two spheres on the form drag coefficients of the front and the rear spheres. The ordinates are the form drag coefficients normalized by those for single spheres. The abscissas are the dimensionless distances between the two spheres. For the front sphere the effect of L/D_A on the form drag coefficients is less considerable as the Reynolds number increases but for the rear sphere the effect becomes much more considerable as the Reynolds number increases. An explanation for this is that for the front sphere the surface pressure is only affected in the lower-half region of the front sphere by the presence of the rear sphere but for the rear sphere the surface pressure in the upper half is much affected by the presence of the front sphere and

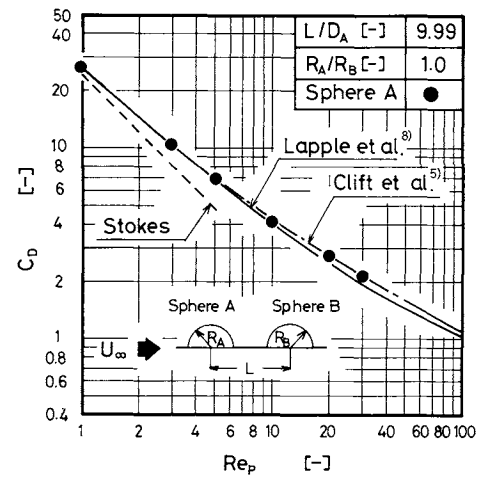

Fig. 2. Drag coefficients of front sphere for the case of large coaxial distance and comparison with those for single sphere.

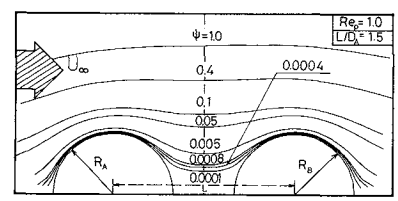

Fig. 3a. Streamlines around two coaxial spheres at $Re_p=1.0$ and $L/D_A=1.50$.

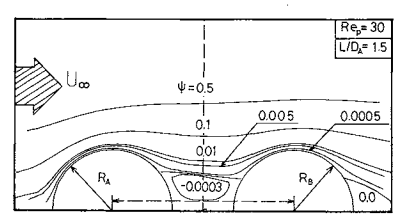

Fig. 3b. Streamlines around two coaxial spheres at $Re_p=30$ and $L/D_A=1.50$.

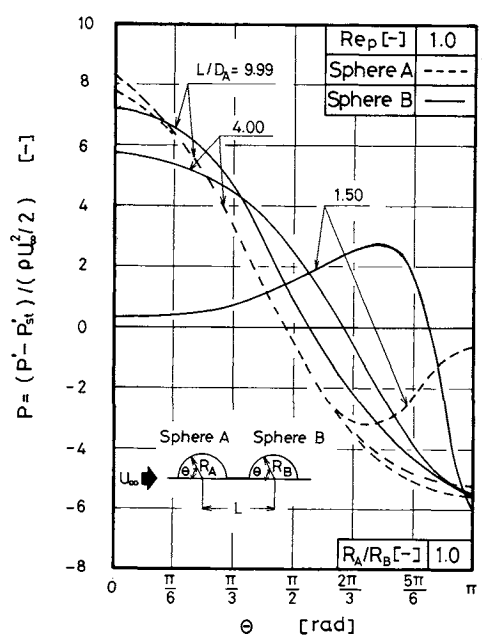

Fig. 4. Local distribution of surface pressure of front and rear spheres at $Re_p=1.0$.

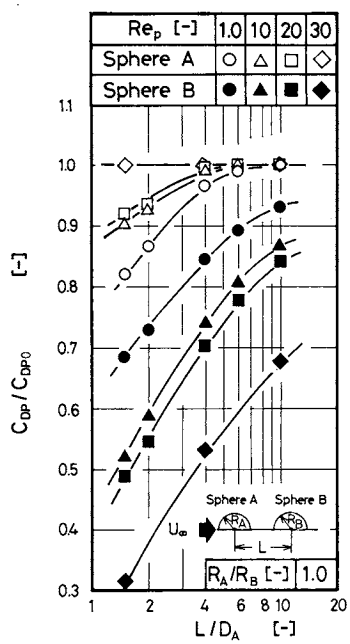

Fig. 5. Form drag coefficients of front and rear spheres.

the effect becomes considerable as the Reynolds number increases.

Figure 6 shows the effect of distances between the two spheres on the friction drag coefficients. The ordinates are the dimensionless friction drag coefficients normalized by those for the single sphere. A similar tendency to that for the form drag coefficients was observed.

Figure 7 shows the effect of the distances between the two spheres on the total drag coefficients of the front and the rear spheres. The ordinates are the total drag coefficients of the front and the rear sphere normalized by those for single spheres. In the figure numerical solutions by Tal *et al.*[15] at $Re_p=40$ are also shown for comparison.

All the numerical data for the total drag coefficients of the front and the rear spheres obtained by the present calculation were successfully correlated by the following equations.

Front sphere:

$$\frac{C_D}{C_{D0}}=\frac{1.0}{1.0+0.32\left(\dfrac{L}{D_A}\right)^{-1.40\cdot Re_p^{0.42}}} \tag{30}$$

Rear sphere:

$$\frac{C_D}{C_{D0}}=\frac{1.0}{\left\{0.53\left(\dfrac{L}{D_A}\right)^{-0.90\cdot Re_p^{0.06}}\right\}\cdot Re_p^{0.31}+1.0} \tag{31}$$

with maximum deviation less than 5%. The ranges of the variables for the correlations are:

$$Re_p=1.0\text{–}30$$

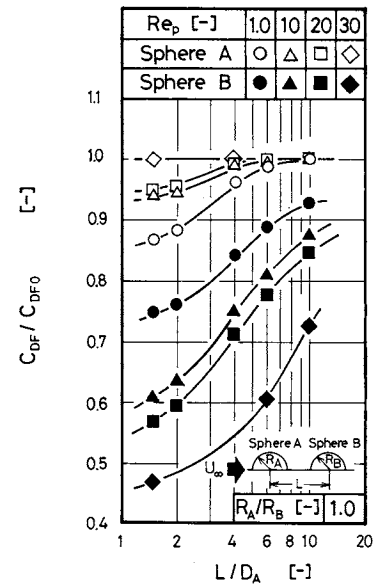

Fig. 6. Friction drag coefficients of front and rear spheres.

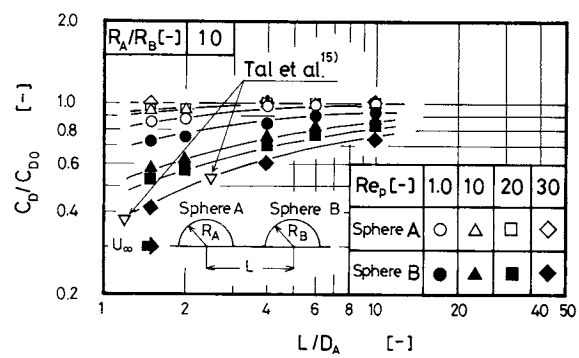

Fig. 7. Total drag coefficients of front and rear spheres.

$$L/D_A=1.5\text{–}9.99$$

$$R_A/R_B=1.0$$

The solid lines in Fig. 7 represent the correlation of the effect of the distance between the two spheres on the total drag coefficients.

3. Mass Transfer for Two Coaxially Arranged Solid Spheres

3.1 Local distribution of the diffusion fluxes

Figure 8(a) shows local distributions of the surface diffusion fluxes of the front and the rear sphere at $Re_p=1$. The ordinates are the dimensionless diffusion fluxes normalized by those at the front stagnation point for the single spheres.[4] For the front sphere the diffusion fluxes in the lower-half region are slightly affected by the presence of the rear sphere, but for the rear sphere the diffusion fluxes are much affected by the presence of the front sphere in the upper-half region, which takes a major role in mass transfer in single spheres, and the effect is considerable as the distances between the two spheres becomes small. A similar tendency is observed for those at $Re_p=30$ as shown in **Fig. 8(b)**.

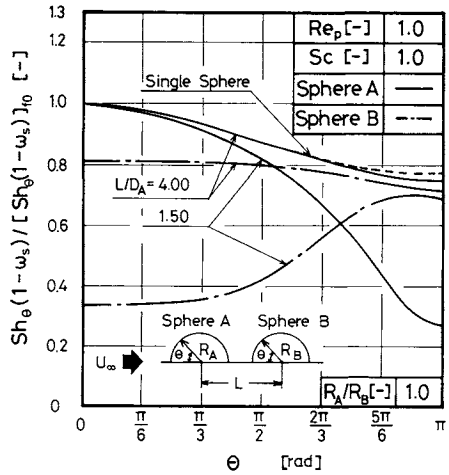

Fig. 8a. Local distribution of diffusion fluxes of front and rear spheres at $Re_p = 1.0$.

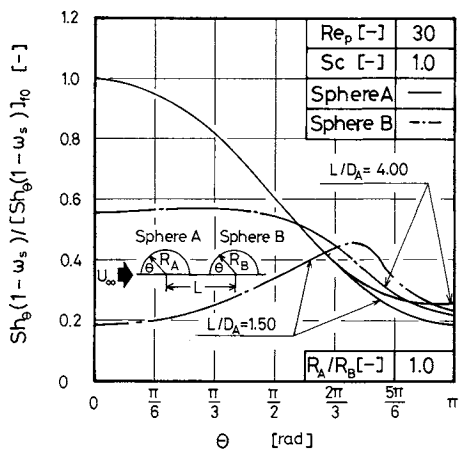

Fig. 8b. Local distribution of diffusion fluxes of front and rear spheres at $Re_p = 30$.

3.2 Average diffusion fluxes and correlation for the effect of two adjacent evaporating drops

Figure 9 shows the effect of the distances between the two spheres on the average diffusion fluxes of the front and the rear sphere. The ordinates are the average diffusion fluxes normalized by those for the single sphere.[4] For the front sphere the effect of L/D_A is rather mild and the diffusion fluxes approach those for the single sphere as the Reynolds number increases. For the rear sphere the effect becomes much more considerable as Reynolds number increases. An explanation for this may well be seen from Figs. 8(a) and (b), where for the front sphere local fluxes in the lower-half region are slightly affected by the presence of the rear sphere whereas for the rear sphere the local fluxes in the upper-half region, which takes a major part in mass transfer in the single sphere, are much affected by the presence of the front sphere.

The present numerical data are well correlated by the following equations.

Front sphere:

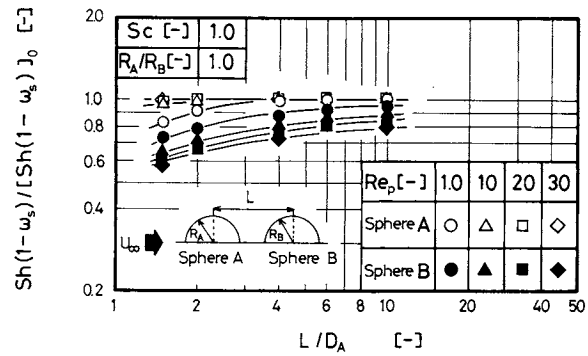

Fig. 9. Average diffusion fluxes of front and rear spheres.

$$\frac{Sh(1-\omega_s)}{[Sh(1-\omega_s)]_0} = \frac{1.0}{1.0+0.67\left(\frac{L}{D_A}\right)^{-3.0\cdot Re_p^{0.40}}} \tag{32}$$

Rear sphere:

$$\frac{Sh(1-\omega_s)}{[Sh(1-\omega_s)]_0} = \frac{1.0}{1.0+0.77\left(\frac{L}{D_A}\right)^{-1.38\cdot Re_p^{-0.26}}} \tag{33}$$

with maximum deviation less than 3%. The ranges of variables for the correlations are:

$$L/D_A = 1.5\text{–}9.99$$

$$Re_p = 1.0\text{–}30$$

$$Sc = 1.0$$

$$R_A/R_B = 1.0$$

The solid lines in Fig. 9 represent the correlation of the effect of the distance between the two spheres on the diffusion fluxes.

3.3 Comparison of numerical data with observed data for evaporation of a pendant water drop

An exact comparison of the present numerical data with observed data is rather difficult because of technical difficulties in measuring rates of evaporation of two coaxially arranged evaporating drops. As for a rough comparison, evaporation of a pendant water drop by air for the case with a coaxially arranged solid sphere in front of an evaporating drop at $Re_p = 30$ with the same apparatus used in our previous work[2] was carried out and compared with the present numerical data.

Figure 10 shows the results of the comparison. The solid line in the figure represents the prediction by Eq. (33) at $Re_p = 30$ and the solid circle is the numerical solution for the diffusion flux of the rear sphere behind the coaxially arranged inert solid sphere (without mass flux) at $Re_p = 30$. Good agreement between these is observed. For comparison, an empirical correlation for the intermediate Reynolds number range ($Re_p = 53\text{–}370$) by the authors,[2] an empirical correlation by Miura *et al.*,[10] numerical solutions at $Re_p = 40$ by Tal *et al.*[15] and numerical solutions by

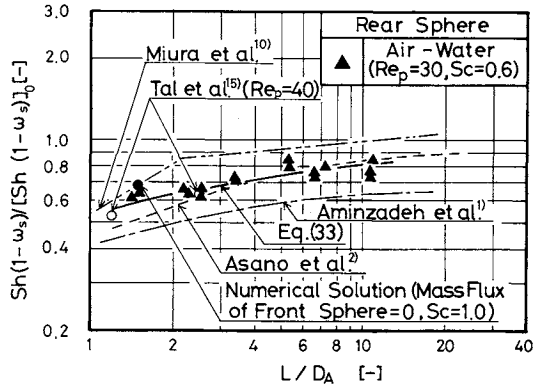

Fig. 10. Effect of distance between two spheres on diffusion fluxes of front and rear spheres; comparison with observed data at $Re_p = 30$.

Aminzadeh *et al.*[1] are also shown in the figure.

Considering the fact that the order of magnitude of Reynolds number is less than 30 for spray drying, the proposed correlations may well be applied to practical use.

Conclusions

Numerical analysis for drag coefficients and mass transfer of two coaxially arranged spheres was made by use of a finite difference method with bipolar coordinate system for $Re_p = 1$–30, $L/D_A = 1.5$–9.99 and $Sc = 1$ to give the following conclusions.

1) New correlations for the effect of distances between the two spheres on the drag coefficients and the diffusion fluxes of the front and the rear spheres were proposed.

2) The proposed correlation for the diffusion fluxes of the rear sphere showed good agreement with the observed data for evaporation of a pendant water drop by air.

Appendix

Equations (1) and (11) can be further simplified by introducing the following function:

$$G = \frac{\zeta \cdot \sin\xi}{(\cosh\eta - \cos\xi)} \tag{A-1}$$

Hence Eqs. (1) and (11) are reduced to the following forms:

$$\sin\xi \cdot (\cosh\eta - \cos\xi) \cdot \left(\frac{\partial\psi}{\partial\eta}\cdot\frac{\partial}{\partial\xi} - \frac{\partial\psi}{\partial\xi}\cdot\frac{\partial}{\partial\eta}\right) \cdot \left\{\frac{(\cosh\eta - \cos\xi)^2}{\sin^2\xi}\cdot G\right\} = \frac{1}{Re_c}E^2 G \tag{A-2}$$

$$E^2\psi = G \tag{A-3}$$

The finite difference forms of Eqs. (A-2), (A-3) and (3) are as follows:

$$\psi^n_{i,j} = \frac{1}{2(\cosh\eta - \cos\xi)}\cdot\left\{\frac{(\Delta\eta)^2\cdot(\Delta\xi)^2}{(\Delta\xi)^2 + (\Delta\eta)^2}\right\} \times\left[\left\{\frac{2(\cosh\eta - \cos\xi) + \Delta\eta\sinh\eta}{2(\Delta\eta)^2}\right\}\psi^n_{i+1,j} + \left\{\frac{2(\cosh\eta - \cos\xi) - \Delta\eta\sinh\eta}{2(\Delta\eta)^2}\right\}\psi^n_{i-1,j} + \left\{\frac{(2\sin\xi - \Delta\xi\cos\xi)\cosh\eta - \sin 2\xi + \Delta\xi}{2(\Delta\xi)^2\sin\xi}\right\}\psi^n_{i,j+1} + \left\{\frac{(2\sin\xi + \Delta\xi\cos\xi)\cosh\eta - \sin 2\xi - \Delta\xi}{2(\Delta\xi)^2\sin\xi}\right\}\psi^n_{i,j-1} - \frac{1}{\cosh\eta - \cos\xi}G^n_{i,j}\right] \tag{A-4}$$

$$G^{n+1}_{i,j} = \frac{1}{2(\cosh\eta - \cos\xi)}\cdot\frac{(\Delta\eta)^2(\Delta\xi)^2}{(\Delta\eta)^2 + (\Delta\xi)^2} \times\left[\left\{\frac{2(\cosh\eta - \cos\xi) + \Delta\eta\sinh\eta}{2(\Delta\eta)^2}\right\}G^n_{i+1,j} + \left\{\frac{2(\cosh\eta - \cos\xi) - \Delta\eta\sinh\eta}{2(\Delta\eta)^2}\right\}G^n_{i-1,j} + \left\{\frac{(2\sin\xi - \Delta\xi\cos\xi)\cosh\eta - \sin 2\xi + \Delta\xi}{2(\Delta\xi)^2\sin\xi}\right\}G^n_{i,j+1} + \left\{\frac{(2\sin\xi + \Delta\xi\cos\xi)\cosh\eta - \sin 2\xi - \Delta\xi}{2(\Delta\xi)^2\sin\xi}\right\}G^n_{i,j-1}\right] - \frac{Re_c(\cosh\eta - \cos\xi)}{8\sin\xi}\cdot\frac{(\Delta\eta)(\Delta\xi)}{(\Delta\xi)^2 + (\Delta\eta)^2} \times\{(\psi^n_{i+1,j} - \psi^n_{i-1,j})(G^n_{i,j+1} - G^n_{i,j-1}) - (\psi^n_{i,j+1} - \psi^n_{i,j-1})(G^n_{i+1,j} - G^n_{i-1,j})\} + \frac{Re_c G^n_{i,j}}{\sin^2\xi}\cdot\frac{(\Delta\eta)^2(\Delta\xi)^2}{(\Delta\xi)^2 + (\Delta\eta)^2} \times\left[(\cosh\eta\cos\xi - 1)\left\{\frac{\psi^n_{i+1,j} - \psi^n_{i-1,j}}{2(\Delta\eta)}\right\} + \sin\xi\sinh\eta\left\{\frac{\psi^n_{i,j+1} - \psi^n_{i,j-1}}{2(\Delta\xi)}\right\}\right] \tag{A-5}$$

$$\theta^{k+1}_{c_{i,j}} = \frac{(\Delta\eta)^2(\Delta\xi)^2}{2\{(\Delta\eta)^2 + (\Delta\xi)^2\}}\left[\left\{\frac{1}{(\Delta\eta)^2} - \frac{\sinh\eta}{2(\Delta\eta)(\cosh\eta - \cos\xi)} + \frac{(\cosh\eta - \cos\xi)Re_c Sc}{4(\Delta\eta)(\Delta\xi)\sin\xi}\cdot(\psi_{i,j+1} - \psi_{i,j-1})\right\}\theta^k_{c_{i+1,j}} + \left\{\frac{1}{(\Delta\eta)^2} + \frac{\sinh\eta}{2(\Delta\eta)(\cosh\eta - \cos\xi)} - \frac{(\cosh\eta - \cos\xi)Re_c Sc}{4(\Delta\eta)(\Delta\xi)\sin\xi}\cdot(\psi_{i,j+1} - \psi_{i,j-1})\right\}\theta^k_{c_{i-1,j}} + \left\{\frac{1}{(\Delta\xi)^2} + \frac{\cos\xi\cosh\eta - 1}{2(\Delta\xi)\sin\xi(\cosh\eta - \cos\xi)} - \frac{(\cosh\eta - \cos\xi)Re_c Sc}{4(\Delta\eta)(\Delta\xi)\sin\xi}\cdot(\psi_{i+1,j} - \psi_{i-1,j})\right\}\theta^k_{c_{i,j+1}} + \left\{\frac{1}{(\Delta\xi)^2} - \frac{\cos\xi\cosh\eta - 1}{2(\Delta\xi)\sin\xi(\cosh\eta - \cos\xi)} + \frac{(\cosh\eta - \cos\xi)Re_c Sc}{4(\Delta\eta)(\Delta\xi)\sin\xi}\cdot(\psi_{i+1,j} - \psi_{i-1,j})\right\}\theta^k_{c_{i,j-1}}\right] \tag{A-6}$$

Nomenclature

C_D = total drag coefficient [—]

C_{DF}	=	friction drag coefficient	[—]
C_{DP}	=	form drag coefficient	[—]
c	=	focal length of bipolar coordinate system	[m]
D_A, D_B	=	diameter of front or rear sphere	[m]
$\mathscr{D}$	=	binary diffusion coefficient	[m²/s]
E^2	=	operater defined by Eq. (2)	[—]
L	=	distance between centers of two spheres	[m]
M	=	number of mesh points in the η direction	[—]
N	=	number of mesh points in the ξ direction	[—]
P	=	dimensionless pressure $(=(P'-P'_{st})/1/2\rho U_\infty^2)$	[—]
P'_{st}	=	static pressure of free stream	[Pa]
R_A, R_B	=	radius of front or rear sphere	[m]
R_∞	=	dimensionless distance defined by Eq. (13)	[—]
R'_∞	=	dimensional distance from median point connecting two spheres to outer boundary	[m]
Re_c	=	Reynolds number defined by Eq. (9d)	[—]
Re_p	=	Reynolds number $(=D_A U_\infty/\nu)$	[—]
Sc	=	Schmidt number $(=\nu/\mathscr{D})$	[—]
Sh	=	Sherwood number defined by Eqs. (26), (27)	[—]
U_∞	=	free stream velocity	[m/s]
X	=	x component of rectangular coordinate	[m]
Y	=	y component of rectangular coordinate	[m]
Δ	=	difference	[—]
$\varepsilon_1, \varepsilon_2$	=	allowable maximum error in convergence criterion	[—]
ζ	=	vorticity defined by Eq. (11)	[—]
η	=	bipolar coordinate, normal to ξ	[—]
θ	=	angle from forward stagnation points	[rad]
θ_c	=	dimensionless concentration $(=(\omega-\omega_\infty)/(\omega_s-\omega_\infty))$	[—]
ν	=	kinematic viscosity of gas	[m²/s]
ξ	=	bipolar coordinate, angle	[rad]
ρ	=	density	[kg/m³]
ψ	=	dimensionless stream function	[—]
ω	=	mass fraction	[—]

〈Subscripts〉

A	=	front sphere
B	=	rear sphere
f	=	front stagnation point
i	=	mesh point in η direction
j	=	mesh point in ξ direction
s	=	surface of sphere
∞	=	free stream
θ	=	local value in θ direction
0	=	single sphere

〈Superscript〉

k	=	number of iteration
n	=	number of iteration

Literature Cited

1) Aminzadeh, K., T. R. Al Taha, A. R. H. Cornish, M. S. Kolansky and R. Pfeffer: *Int. J. Heat Mass Transfer*, **17**, 1425 (1974).
2) Asano, K., I. Taniguchi and H. Nishimura: *Kagaku Kogaku Ronbunshu*, **12**, 583 (1986).
3) Chuchottaworn, P., A. Fujinami and K. Asano: *J. Chem. Eng. Japan*, **16**, 18 (1983).
4) Chuchottaworn, P., A. Fujinami and K. Asano: *J. Chem. Eng. Japan*, **17**, 1 (1984).
5) Clift, R., J. R. Grace and M. E. Weber: "Bubbles, Drop and Particles," p. 142–168, Academic Press, New York (1978).
6) Happle, J. and H. Brenner: "Low Reynolds Number Hydrodynamics," p. 96–158, Prentice-Hall, Inc., Englewood Cliffs (1965).
7) Labowsky, M.: *Chem. Eng. Sci.*, **31**, 803 (1976).
8) Lapple, C. E. and C. B. Shepherd: *Ind. Eng. Chem.*, **32**, 605 (1940).
9) Marberry, M., A. K. Ray and K. Leung: *Combust. Flame*, **57**, 237 (1984).
10) Miura, K., T. Miura and S. Ohtani: *Kagaku Kogaku Ronbunshu*, **1**, 241 (1975).
11) Ramachandran, S. and C. Kleinstreuer: *Chem. Eng. Commun.*, **36**, 197 (1985).
12) Ray, A. K. and E. J. Davis: *Chem. Eng. Commun.*, **6**, 61 (1980).
13) Roache, P. J.: "Computational Fluid Dynamics," Hermosa Publishers Inc., Albuquerque, New Mexico (1976).
14) Stimson, M. and G. B. Jeffery: *Proc. Roy. Soc. (London)*, **A111**, 110 (1926).
15) Tal, R., D. N. Lee and W. A. Sirignano: *Int. J. Heat Mass Transfer.*, **27**, 1953 (1984).
16) Umemura, A., S. Ogawa and N. Oshima: *Combust. Flame*, **41**, 35 (1981).